ELSEVIER

Journal of Nuclear Materials 250 (1997) 118–130

journal of nuclear materials

Calculation of used nuclear fuel dissolution rates under anticipated Canadian waste vault conditions

S. Sunder *, D.W. Shoesmith, M. Kolar, D.M. Leneveu

Atomic Energy of Canada Ltd., Whiteshell Laboratories, Pinawa, MB, Canada ROE 1LO

Received 11 February 1997; accepted 27 August 1997

Abstract

Dissolution rates of UO_2 fuel are determined as a function of alpha and gamma dose rates. These room-temperature rates are used to calculate the dissolution rates of used fuel at 100°C. Also, the alpha, beta and gamma dose rates in water in contact with the reference used fuel are calculated as a function of cooling time. These results are used to calculate used CANDU fuel dissolution rates as a function of time since emplacement in a defective copper container for the Canadian Nuclear Fuel Waste Management Program. It is shown that beta radiolysis of water is the main cause of oxidation of used CANDU fuel in a failed container and that the use of a corrosion model is required for ~ 1000 a of emplacement in the waste vault. The results obtained here can be adopted to calculate used nuclear fuel dissolution rates for other waste management programs. © 1997 Elsevier Science B.V.

1. Introduction

The concept of direct disposal of used nuclear fuel in a geological disposal vault is being considered in several countries [1–24]. The concept envisages sealing the used nuclear fuel in corrosion-resistant containers that would then be placed in a deep geological disposal vault. In a recent case study for the Canadian Nuclear Fuel Waste Management Program (CNFWMP) [24], it is assumed that the fuel will be placed in 25 mm thick copper containers. Since the predicted lifetimes of these containers are $> 10^6$ a, only those containers emplaced with an undetected defect need to be considered in a safety analysis. It has been estimated that between 1 in 10^4 and 1 in 10^3 containers would contain defects capable of causing early failures [25,26]. Although entry of water into the containers will not begin immediately on failure, since locally unsaturated conditions are expected in the vicinity of the containers, it is judicious to assume that complete flooding would occur instantaneously. Since the fuel cladding is assumed not to act as a barrier in any manner, this would lead to immediate wetting of the fuel with oxidizing groundwater. This groundwater will be oxidizing because of (a) dissolved oxygen from the air trapped in the container, (b) oxygen that diffuses into the container once it has failed and (c) the products of water radiolysis caused by the ionizing radiation associated with the radionuclides in the fuel [14,15]. Here, we present a model to calculate fuel dissolution rates under these conditions, i.e., in a rapidly failed copper container.

2. Model for used fuel dissolution

In a previous case study for the CNFWMP [16,17], the model for UO_2 fuel dissolution was assumed to be limited by the solubility of UO_{2+x} (up to U_4O_9) and the diffusional transport of dissolved uranium away from the surface of the fuel. The solubility of uranium was calculated using a thermodynamic model by sampling from a range of concentrations of groundwater species and E_h (oxidation potential) and pH values [27]. This model is applicable providing E_h is not positive to the U_4O_9/U_3O_7 boundary [17]. However, any model of fuel dissolution within a

* Corresponding author. Present address: Research Chemistry Branch, Chemistry and Chemical Eng. Div., Chalk River Laboratories AECL, Chalk River, Ont., Canada K0J 1J0. Fax: +1-613 584 1220; e-mail: sunders@aecl.ca.

PII S0022-3115(97)00272-9

prematurely failed container must take into account the fact that, initially, the redox conditions will be oxidizing, due to the presence of dissolved oxygen and the production of oxidizing radiolysis products. Under these conditions, oxidation beyond the U_4O_9/U_3O_7 boundary is inevitable and the dissolution rate will be determined by kinetic factors making the use of a thermodynamically-based model inappropriate [13].

There is a large body of evidence demonstrating that, for more oxidizing conditions, the dissolution of fuel must be considered as an electrochemical process and therefore treated kinetically [5,28]. The dissolution reaction of UO_2 is a coupled process under oxidizing conditions involving the oxidative dissolution of the UO_2 and the reduction of the available oxidant:

$$UO_2 \rightarrow UO_2^{2+} + 2e^- \quad (1)$$

$$Ox + ne^- \rightarrow Red. \quad (2)$$

Depending on the relative kinetics of these two half reactions, the dissolving surface will adopt a potential, known as the corrosion potential (E_{corr}), between the equilibrium values for these two reactions (Fig. 1). Under these conditions, dissolution will occur with both reactions away from equilibrium, and the fuel can be said to be undergoing corrosion. As corrosion proceeds, the increase in the surface concentration of dissolved uranium will lead to an increase in the equilibrium potential of the surface reaction, and the consumption of the oxidant will cause a fall in the value of $E_{ox/red}$; i.e., the potential difference driving the corrosion reaction will decrease as oxidant is consumed. Consequently, if available oxidants are consumed, and not replenished, and corrosion products accumulate in the vicinity of the fuel surface, the need for a model based on the kinetics of the corrosion process will diminish. Providing the potential difference across the solid/solution interface (i.e., the difference in equilibrium potential for the two half reactions) is eventually reduced to zero, then the reapplication of the solubility-based, transport-limited dissolution model would be appropriate. The overall fuel reaction is appropriately considered as a corrosion reaction when $E_h > E_{corr}$ but as a dissolution reaction when $E_h \sim E_{corr}$. We conservatively assume that equilibrium would never be established as redox conditions evolve but assume that a constant corrosion rate will persist even at long times.

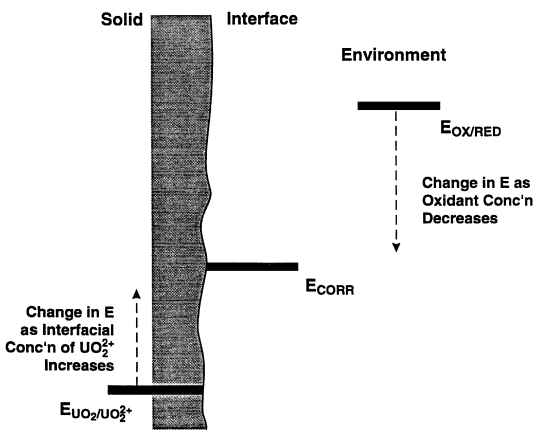

Fig. 1. Relationship between potentials when the surface of the fuel is not in equilibrium with its environment and an electrochemical driving force for corrosion exists.

3. Evolution of redox conditions in the failed container

The evolution in redox conditions within the container will be determined by the sum effects of oxygen consumption and the decay of radiation fields within the fuel. The oxygen concentration will decrease at a rate determined by its rate of consumption by the fuel and by other oxidizable materials in the container, especially the copper walls of the container itself. The gamma-, beta- and alpha-radiation fields at the surface of the fuel will decay with time at a rate determined by the nature of the fuel and its in-reactor history [29,30]. Radiolytically produced oxidants could also be consumed by reaction with the copper container. For alpha and beta radiolysis, oxidants will be produced locally at the fuel surface and must be transported to the walls of the container [30–32]. For gamma radiolysis, the production of oxidants will be more widely dispersed. As these oxidants are consumed, redox conditions will become controlled by a complex suite of redox reactions involving the products of corrosion processes (on copper (Cu^I/Cu^{II} species) and any iron-containing structural components (Fe^{II}/Fe^{III} species) within the container) and the oxidized products of fuel corrosion (U^{VI} species).

4. Calculation of fuel dissolution rates

In this report we calculate the fuel corrosion rates based on our recently developed electrochemical model [5]. In this model the rates are predicted as a function of redox conditions by extrapolating steady-state electrochemical currents for the anodic dissolution of UO_2 to the corrosion potentials measured in solutions undergoing radiolysis or containing the various available oxidants.

These corrosion (dissolution) rates are then combined with a knowledge of the evolution of redox conditions within the container to predict the change in fuel corrosion rate with time. This requires that the rate of consumption of oxygen and the radiation decay profile as a function of age of the fuel be known, as shown schematically in Fig. 2. Once the electrochemical driving force disappears (Fig. 1) then the rate of corrosion will fall to a low value. Below this threshold value of the corrosion rate (Fig. 2C), the

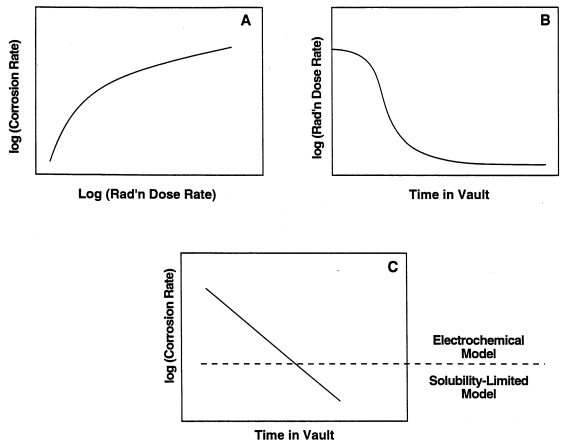

Fig. 2. Illustration of the procedure used to determine fuel corrosion rates as a function of time in the vault (C) from a knowledge of corrosion rates as a function of radiation dose rate (A) and the calculated radiation dose rate decay curves (B) (Fig. 3). The horizontal dashed line in (C) denotes the threshold value of the chemical dissolution rate.

process can be considered as a dissolution reaction, and a solubility-based, transport-limited model would be as appropriate as an electrochemical one [5], although we have chosen to continue using the more conservative corrosion rate-based model, as discussed above (Section 2).

4.1. Corrosion due to dissolved oxygen

The amount of oxygen available to cause corrosion of the fuel can be calculated from the volume of air originally trapped within the container. This assumes no more oxygen will diffuse into the container through the small defect since corrosion of the outside of the container will rapidly reduce the concentration of oxygen close to its surface to a small value [33].

The inventory of available oxygen has been calculated to be 1.01 mol based on the amount of oxygen trapped in the void volume (118 l) within the container (see appendix C in Ref. [24]). If all of this oxygen were to cause oxidation of the fuel according to the reaction

$$UO_2 + \tfrac{1}{2}O_2 = UO_3 \qquad (3)$$

then the maximum amount of fuel oxidized would be about 2.016 mol ($\sim$ 544 g) of UO_2. Since a container will contain 72 bundles, each comprising 21.3 kg of fuel, this amounts to only a very small fraction (0.00035) of the 1534 kg of fuel. A possibility is that the oxygen could be used in the dry oxidation of the fuel prior to wetting. This can be shown to be very slow [34] and would not significantly affect the subsequent rate of fuel dissolution [19].

While the available oxygen can only cause a limited amount of fuel oxidation, the presence of dissolved oxygen while radiation fields endure, especially gamma and beta, can lead to a significant increase in the rate of fuel corrosion due to the production of the oxidizing products of water radiolysis [5,10,11,15]. To determine whether this effect need be considered, we have calculated the relative rates of oxygen consumption by corrosion of the fuel and by corrosion of the copper container (Appendix A). This comparison shows that the rate of consumption by reaction with copper is $\sim 10^4$ times higher than that by reaction with UO_2 leading to the consumption of most of the oxygen in the container in $\sim$ 1.4 days (Appendix A).

Since the oxygen will be rapidly consumed by the copper container we need only consider corrosion driven by the radiolysis of deaerated solutions. This is a significant advantage since the predicted corrosion rates in deaerated solutions are much lower than in oxygenated solutions [5,10].

4.2. Radiation dose rates for used fuel as a function of time

The radiolysis of water produces both molecular and radical oxidants and reductants [14,31,32], and the concentration of the different species formed depends on both the nature of the ionizing radiation and the dose rate to the water. It is well known that low linear energy transfer (LET) radiation (beta and gamma) produces more radicals (e.g., H, OH) than high LET radiation (alpha) which results predominantly in the formation of molecular radiolysis products (e.g., H_2O_2). The consumption of these radiolytic oxidants by reaction with the container will not prevent radiolytically induced corrosion of the fuel. Due to the short range of alpha and beta particles in water, they will only produce oxidants close to the fuel surface, and the radicals (the main oxidants formed by gamma and beta radiolysis) are too reactive to escape the reaction layer at the fuel surface [35].

To evaluate the effects of water radiolysis on the fuel corrosion rate, it is necessary to know the dose rate to the

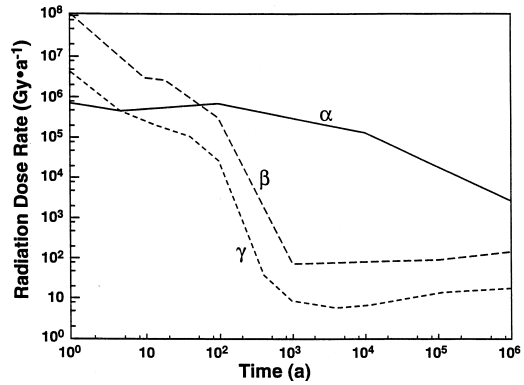

Fig. 3. Alpha, beta and gamma dose rates in the water layer in contact with the reference fuel, used CANDU fuel with a burnup of 721 GJ/kg U, as a function of cooling time.

water in the container due to the different types of ionizing radiation. Here, we consider the effects of beta and gamma radiation together since both are low LET radiations. Fig. 3 shows alpha, beta and gamma dose rates in water in contact with the reference used fuel (burnup of 721 GJ (kg U)$^{-1}$) for a *single* fuel bundle, as a function of time. These results are obtained using the procedure and data described elsewhere [30]. Since alpha and beta radiations produce oxidants only in the vicinity of the surface from which they are emitted, their dose rates are independent of the number of fuel bundles in the container. However, for gamma radiation the irradiation of adjacent surfaces will occur and the dose rate to the water at the fuel surface will depend both on the number of fuel bundles in the container and on their placement geometry. We estimate that the average gamma dose rate in the container will be about 4 to 7 times that calculated for a single bundle in Fig. 3 (see appendix G in Ref. [24]).

4.3. Corrosion rates used in the model

Since the oxygen within the container will be consumed rapidly, only the corrosion rates due to the radiolysis of deaerated solutions need be used to predict radionuclide release rates. Fig. 4 shows these rates as a function of gamma [5,10,11] and alpha [20] dose rates at room temperature (22°C). The data used in these figures were recorded in 0.1 mol l^{-1} $NaClO_4$ (pH = 9.5), a solution typical of the non-complexing groundwaters expected under waste

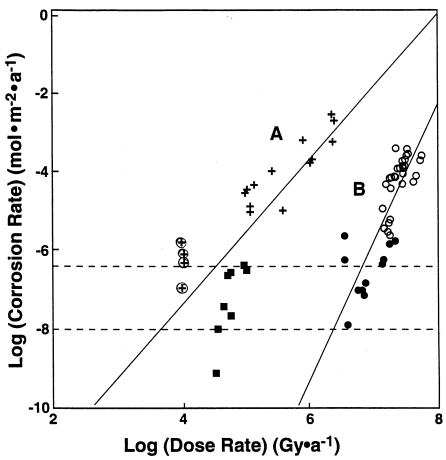

Fig. 4. Fuel corrosion rates for neutral non-complexing solutions (0.1 mol l^{-1} $NaClO_4$; pH = 9.5) at room temperature (~ 22°C). The results for gamma radiolysis (A) are from Shoesmith and Sunder [5] and those for alpha radiolysis (B) from Sunder et al. [20]. The straight lines correspond to a fit to all the data (Appendix C). The upper and lower horizontal lines show the predicted corrosion rates for corrosion potentials of −100 and −200 mV (vs. SCE), respectively. The solid data points (■ and ●) are those not subsequently used in predicting fuel dissolution rates. The points indicated by the symbol ⊕ are dubious experimental points (see Appendix C).

vault conditions, and have been published elsewhere [5,20]. We assume that the corrosion rates due to beta radiolysis are the same as those due to gamma radiolysis since both are low LET radiations (Section 4.2). The rates for alpha radiolysis shown in Fig. 4 are from experiments carried out in crevices 30 μm in width and are, therefore representative of the behavior expected in narrow cracks in the fuel or at the fuel/cladding interface.

The upper horizontal dashed line in Fig. 4 represents the corrosion rate (3.52×10^{-7} mol m^{-2} a^{-1}) predicted by our model for a corrosion potential of −100 mV (vs. SCE), the potential at which our electrochemistry/XPS results tell us the surface composition is $UO_{2.33}$ [11,13]. Above this value, the $UO_{2.33}$ film achieves a constant thickness and, under steady-state conditions, the rate of its formation is balanced by the rate of its oxidative dissolution; i.e., steady-state corrosion conditions are achieved [36]. Below this potential, the degree of oxidation of the surface is determined by the potential achieved, and a state of redox equilibrium appears to prevail [13]. Consequently, we have taken this value as a threshold above which the application of a corrosion model, as opposed to a transport-limited solubility-based model, is essential [5]. For values below this threshold, the process should be considered as a dissolution reaction. The lower horizontal line represents the corrosion rate (8.79×10^{-9} mol m^{-2} a^{-1}) predicted by our model for a corrosion potential of −200 mV (vs. SCE), the highest value observed in our experiments in deaerated solutions. Inevitably, corrosion potentials are less than −200 mV on unirradiated UO_2 in deaerated solutions making the value at −200 mV a conservative estimate of the maximum rate of dissolution under deaerated conditions in the absence of any radiation field. We consider this rate to be the lower limit of applicability of our corrosion model. Consequently, the need for a corrosion model disappears once the corrosion rate falls to a value somewhere in the range between these bounding values. In our calculations, once this occurs, we assume that further dissolution of the fuel will continue indefinitely at this constant threshold rate.

An alternative approach once the redox conditions have become sufficiently 'non-oxidizing', and a corrosion model is no longer essential, would be to return to the transport-limited, solubility-based model used in the previous case study [16]. However, the transition from a kinetic to a thermodynamically based approach is complicated and the effort necessary to implement such a transition hard to justify. This is because the corrosion product, U^{VI} (in the form of hydrolyzed UO_2^{2+} species) is not inert but can become involved in redox reactions with various components of the system, particularly the copper container and the products of its corrosion, and any iron/iron oxides. This will lead to a period when the redox potential of the system is buffered by a complex set of reactions, culminating eventually in conditions for which the application of the transport-limited, solubility-based model is appropriate.

In the absence of a much more extensive kinetic database, it is impossible to calculate how long this period of redox adjustment would take.

4.4. The effect of temperature on the corrosion rate

The corrosion rates shown in Fig. 4 were measured at room temperature (~ 22°C) whereas the temperature in the container will be above this value for nearly 10^5 a [37,38]. We have taken the temperature in the container to be a conservatively constant 100°C when calculating the corrosion rate of the fuel driven by the radiolysis of water. However, by the time fuel corrosion rates fall to values below our threshold value (see above), which is expected to occur after a few hundred years, the temperature will have fallen to between 60°C and 50°C. Consequently, we have taken a temperature of 55°C to calculate the threshold dissolution rate.

We have chosen an activation energy of 33.5 kJ mol^{-1} based on our review of activation energies [4] and some recently reported measurements [22]. Our review shows that, in non-complexing solutions the measured activation energies (29 to 34 kJ mol^{-1}) are lower than those recorded for carbonate-containing solutions (42 to 63 kJ mol^{-1}). This undoubtedly reflects the inhibiting effect of oxidized surface films and deposited corrosion products, the values measured in carbonate solutions being closer to the 'real' value for unimpeded corrosion. Since the groundwaters expected to flood the container will be relatively non-complexing for the uranyl ion (UO_2^{2+}) the activation energy we have chosen is the largest reported in non-complexing solution

4.5. Calculation of fuel dissolved in a failed waste container

Fig. 5a and b show the corrosion rates used in our calculations plotted logarithmically as a function of radiation dose rate for a temperature of 100°C. The reasons for using only the limited data sets plotted in Fig. 5a and b in our calculations are discussed in Appendix B. Also shown on these figures are the ranges of gamma, beta and alpha dose rates expected over the first 1000 a assuming the fuel is 10 a old when emplaced in the vault. For alpha radiolysis, to predict used-fuel behavior it is necessary to extrapolate to dose rates lower than those used in experimental measurements (Fig. 5a). For gamma/beta radiolysis, our experimental data cover the high dose rate range expected at short times and extrapolation is only required for the lower dose rates prevailing at longer times. The chosen fits to these data, and the errors associated with their extrapolation, are discussed in Appendix C.

The corrosion rate of fuel inside an instantaneously failed container is calculated by the procedure outlined in Fig. 2 using the fitted relationships for fuel corrosion rates as a function of radiation dose rate (Fig. 5) and the calculated dose rates for alpha, beta and gamma radiation (Fig. 3).

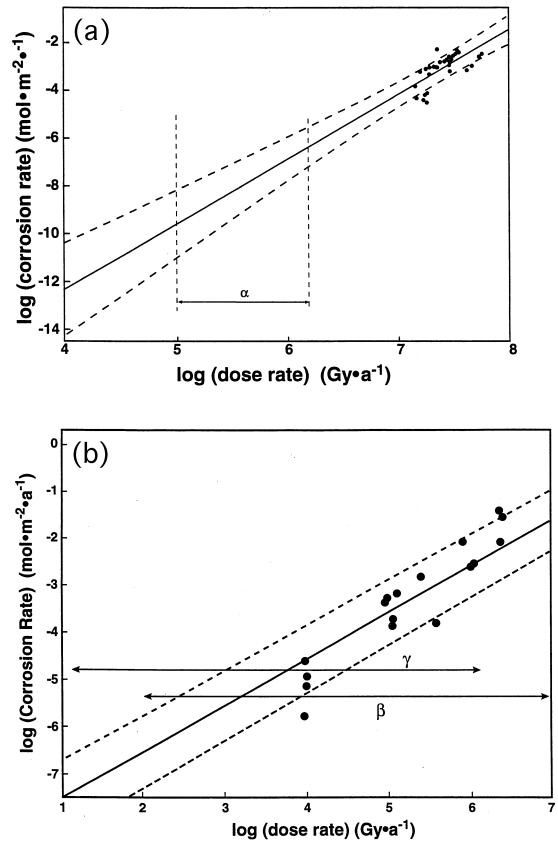

Fig. 5. Fuel corrosion rates calculated for 100°C as a function of radiation dose rate: (a) data for alpha radiolysis; (b) gamma/beta radiolysis. (Note, the eight ■ points from Fig. 4 are not used in (b) and the eleven ● points from Fig. 4 are not used in (a) (Appendix C)). The solid lines are the fitted lines and the dashed lines the $\pm 1\sigma$ values of this fit. The horizontal lines show the range of dose rates between fuel ages of 10 and 1000 a for alpha (α), beta (β) and gamma (γ) radiation, respectively.

The total fuel corrosion rate per unit area of the corroding surface, $c(t)$ (mol m^2 a^{-1}), is given by the sum of the rates due to each radiation source and the threshold dissolution rate value (R_c),

$$c(t) = 10^{b_\alpha}\{\alpha(t+t_c)\}^{a_\alpha} + 10^{b_\beta}\{\beta(t+t_c)\}^{a_\beta} + 10^{b_\gamma}\{F\gamma(t+t_c)\}^{a_\gamma} + R_c, \quad (4)$$

where $\alpha(t)$, $\beta(t)$ and $\gamma(t)$ are the alpha, beta and gamma dose rates to water at the surface of a single fuel bundle, and F is the factor for gamma radiation to convert the dose rate for a single fuel bundle to that expected in the container; $t = 0$ corresponds to the time at which water enters the container and t_c is the time since discharge of the fuel bundle from the reactor. The terms a_α, a_β, a_γ and

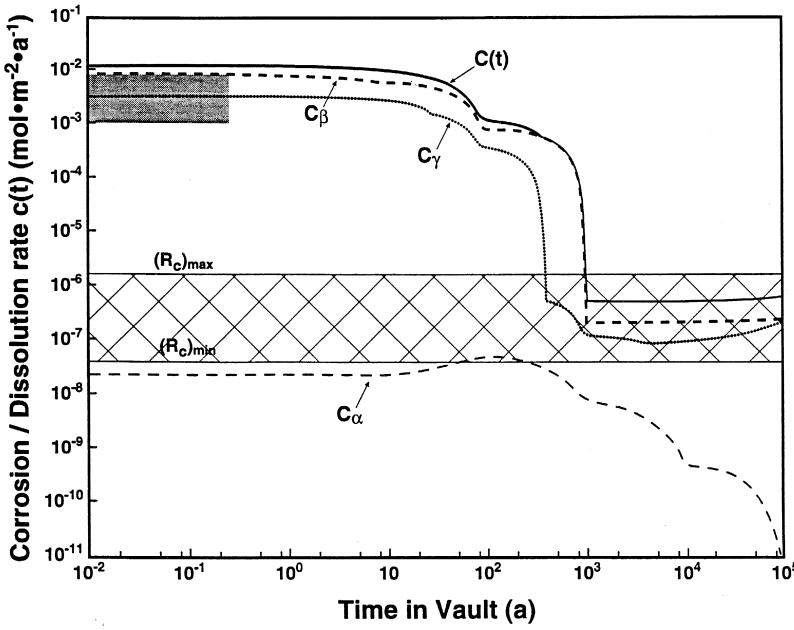

Fig. 6. Predicted corrosion rates for the reference fuel (assuming a constant vault temperature of 100°C) as a function of time of emplacement in the vault assuming the container fails at $t = 0$: (————) total ($c(t)$); (- - -) rate due to β radiolysis (c_β); (· · ·) rate due to gamma radiolysis (c_γ); (— — —) rate due to alpha radiolysis (c_α). The lower cross-hatched area is the range of threshold dissolution rate values. The upper shaded area is the range of temperature-corrected measured fuel corrosion rates (Table 2).

b_α, b_β, b_γ are the fitting parameters for the slopes and intercepts, respectively, of the lines plotted through the data in Fig. 5. The procedure used to fit the data to obtain values of a and b is also described in Appendix C. The range of values for the threshold dissolution rate, R_c, is shown in Fig. 6.

The corrosion rate, $c(t)$ (from Eq. (4)), for ten-year old fuel ($t_c = 10$ a), the range of values for the threshold dissolution rate, R_c, and the breakdown into contributions from alpha, beta and gamma radiolysis are shown in Fig. 6. The values of the parameters used to calculate the rates are given in Table 1. The fraction of used fuel dissolved is shown in Fig. 7.

According to the predictions of Fig. 6, corrosion due to

Table 1
Parameter values used in calculating used fuel dissolution rates in a failed container

Parameter	Symbol	Units	Value[a]
Mass of fuel per container[b]	m	kg	1533.6
Area of fuel per container[b]	A	m^2	306.72
Maximum temperature[b]	T	°C	100
Chemical dissolution rate at 55°C[c]	R_c	mol m^{-2} a^{-1}	2.20×10^{-7}
Alpha fuel dose exponent[d]	a_α		2.7172
Alpha fuel rate convert factor[d]	b_α		−23.1434
Beta fuel rate convert factor[d]	b_β		−8.5426
Gamma fuel rate convert factor[d]	b_γ		−8.5426
Gamma dose vary factor[e]	F		5.5
Gamma fuel dose exponent[d]	a_γ		1

[a] The number of digits does not represent the 'significant digits' but the number used in the SYVAC program to obtain results shown in Figs. 7 and 8.
[b] From Refs. [24,37].
[c] This work, Section 4.5.
[d] This work, Section 4.5, Eq. (4) and Appendix C.
[e] Eq. (4).

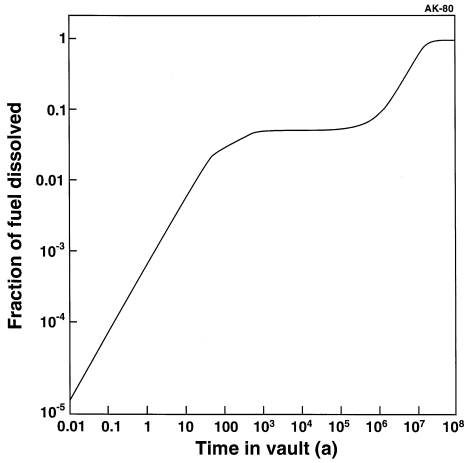

Fig. 7. Fraction of used fuel dissolved calculated for the parameter values in Table 1. For the chemical dissolution rate, R_c, a median value of 2.20×10^{-7} mol m^{-2} a^{-1} was used.

alpha radiolysis will be insignificant since the rate is always less than the range of threshold values for the solubility-limited dissolution rate, shown as the lower shaded area in the figure. By contrast, corrosion rates due to beta and gamma radiolysis are predicted to exceed the threshold value for $\sim$1000 a, due predominantly to the high dose rates for beta radiation for this period (Fig. 3). If we were to consider gamma radiation only, then corrosion rates would fall below the threshold value in 200 to 300 a, consistent with our previous calculations for the effects of gamma radiation only [5].

Also plotted in Fig. 6 is a shaded area (the upper LHS) showing the dissolution rates determined from experimental measurements of used fuel with a burnup of 1110 GJ $(kg\ U)^{-1}$, i.e., higher than that for the reference fuel used in our calculations. The upper bound of this area is the rate at 100°C $(9.4 \pm (4.8)\times10^{-3}$ mol m^{-2} $a^{-1})$ calculated from the rate measured at 22°C in neutral non-complexing solution $(0.54 \pm (0.28)\times10^{-3}$ mol m^{-2} $a^{-1})$ using our activation energy of 33.5 kJ mol^{-1} [4,22]. The lower bound is for a rate one order of magnitude lower. This range represents the uncertainties encountered in measuring the surface area of used fuel specimens [22].

The characteristics of used fuel used in the dissolution rate experiments are compared to those of the reference used fuel considered in our calculations in Table 2. Of greatest importance when attempting to predict the corrosion rate is the sum of the beta and gamma dose rates since it is the oxidants produced by these two processes which have the major influence (the effect of alpha radiolysis is predicted to be negligible). Consequently, we would predict approximately the same corrosion rate for both the reference fuel and the fuel in the dissolution experiments since this sum is nearly the same for both fuels (Table 2). The predicted and experimental values are surprisingly close though this may be fortuitous, since the experimental rate chosen for the comparison is the upper limit of the range of possible rates (shaded area in Fig. 6). If we were to accept a larger value for the surface area of fuel used in dissolution experiments then a lower corrosion rate (within the range shown in Fig. 6) would be obtained, and the margin of overprediction by our model would be greater. A more detailed discussion of the uncertainties in estimating the area of the used fuel is given elsewhere (see Section 4.2 of Ref. [22]).

As expected from the behavior of the dissolution rate with time, the fraction of the fuel dissolved appears to plateau (when plotted logarithmically as in Fig. 7) once the gamma/beta fields have decayed substantially and, as a consequence, the fuel corrosion rate has fallen (Fig. 6). For times $<10^5$ a only 2% of the fuel dissolves. However, if the deviations in the parameter values (listed in Table 1) are taken into account then it is possible that a much larger fraction of the fuel could be dissolved over this period. The total fraction of the fuel dissolved best illustrates the

Table 2
Characteristics of the reference used fuel used for the calculation and that used in the dissolution experiments

Parameter	Reference used fuel	Experimental used fuel
Age (a)	10	11
Burnup $(GJ\ (kg\ U)^{-1})$	720	$\sim$1110
Dose rate $(Gy\ a^{-1})$		
alpha	5.2×10^5	9.39×10^5
beta	3.3×10^6	4.65×10^6
gamma	$1.4\times10^{6\,a}$	$1.2\times10^{4\,b}$
Experimental corrosion rate $(mol\ m^{-2}\ a^{-1})$	—	$9.4 \pm (4.8)\times10^{-3}$
Predicted corrosion rate $(mol\ m^{-2}\ a^{-1})$	13.42×10^{-3}	13.25×10^{-3}

[a] Includes the factor F ($\sim$5.5) to calculate the gamma dose rate in the array of fuel bundles within the container for the reference fuel.
[b] For a used fuel sample of $\sim$0.4 g.

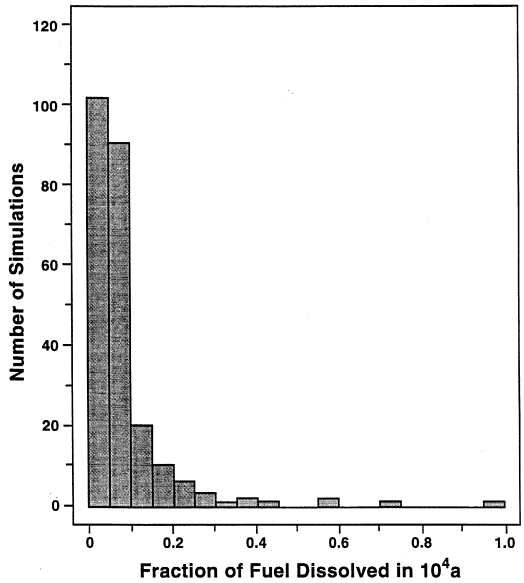

Fig. 8. Distribution of fuel fraction dissolved after 10^4 a of emplacement in the vault determined from 250 simulations of the model using the values of the parameters and their associated errors [24].

sum effect of the uncertainties in the parameters which determine the corrosion rate of the fuel. Fig. 8 shows the distribution of fuel fractions dissolved after 10^4 a of emplacement in the vault determined from 250 simulations of our model. It should be noted here we used a conservative assumption of constant fuel surface area in the calculations to obtain results shown in Fig. 8. This is a good approximation until most of the fuel is consumed. While it is probable that only a small fraction of the fuel will dissolve it is clear that, for the conservatism and parameter uncertainties incorporated in this model, there is a reasonable probability that substantial amounts of fuel could be dissolved at long times.

5. Reliability of predicted corrosion rates

The conclusion that corrosion due to alpha radiolysis is insignificant is based on the empirical relationship that corrosion rate strongly depends on alpha dose rate (the slope (a) of the fitted line in Fig. 5a is 2.7 (Table 1)). As the alpha dose rates for the reference used fuel are 1 to 2 orders of magnitude less than those used experimentally to determine corrosion rates (Fig. 5a), this adds additional uncertainty to the above conclusion. This large slope of 2.7 is not consistent with a simple dependence of corrosion rate on the concentration of oxidants produced by alpha radiolysis. A possibility is that the dependence of corrosion potential on alpha source strength on which these predictions are based is determined by a combination of both corrosion of the fuel and decomposition of the radiolytically produced hydrogen peroxide. If the latter process becomes more dominant at lower source strengths then we would observe a dramatic decrease in corrosion rate as the source strength decreases. This situation has been discussed in more detail elsewhere (e.g., see Refs. [4,5,20,28]), but a thorough understanding remains to be developed.

Experimental measurements to determine corrosion rates due to alpha radiolysis were made in a thin crevice [20] making the concentration of radiolytic oxidants at the fuel surface dependent on the balance between their radiolytic production and their rate of loss by diffusive flux out of the crevice. Intuitively, we would expect this surface concentration to be larger the narrower the width of the crevice since this would reduce their rate of diffusive loss. Consequently, our predictions could underestimate the effects of alpha radiolysis in tight wet cracks in the fuel.

While the agreement between predicted and measured fuel dissolution rates is gratifying, this may be partly fortuitous for a number of reasons. When applying our electrochemical model we chose to extrapolate the highest values of anodic dissolution current recorded. The experimental data show that a less conservatively chosen extrapolation [21] could yield corrosion rate values one to two orders of magnitude lower than those used in our calculations. This, coupled with the uncertainties involved in defining the corrosion rate of used fuel (due to the difficulties in measuring/estimating surface areas), shows that considerable uncertainties still exist in predicted corrosion rate values. A major problem in defining both electrochemical dissolution currents and used fuel corrosion rates in neutral non-complexing solutions is the unpredictable accumulation of corrosion products (e.g., $UO_3 \cdot 2H_2O$) on the dissolving/corroding surface, and the extent to which they block the corrosion process [4,21,22,28].

According to Fig. 7, calculated using the mean values of parameters, all the fuel would be dissolved in $\sim 10^7$ a. However, taking into account the uncertainties in the parameter values would lead to a reasonable probability that all the fuel would be dissolved in $< 10^6$ a. This seems unrealistically rapid for a system in which non-oxidizing conditions should be relatively quickly established and is at odds with expectations based on natural analog studies [39]. While our model contains many conservatisms which, if relaxed, would substantially decrease the predicted fuel dissolution rates and fractions dissolved, it is the values of predicted rates for times greater than 10^3 a which are predominantly responsible for such extensive dissolution.

There are good grounds to believe that our predictions significantly overestimate the rates at long times. Firstly, in predicting the influence of gamma (and hence beta) radiolysis we ignored the decrease in rate at low dose rates (Fig. 4 and Appendix C). If this decrease was to be incorporated into our model then the dissolution rates predicted for gamma and beta radiolysis would decrease

substantially as the dose rate decayed to $< 10^5$ GJ a^{-1}; i.e., after $\sim$ 1000 a (Fig. 3). Secondly, the real decrease in rate expected when conditions become non-oxidizing is avoided by assuming the threshold values used (Fig. 6 and Table 1).

6. Applicability to other fuels

The dissolution rate vs. dose rate relationships derived here are also applicable to used fuels other than CANDU fuel provided the contact with water occurs under anaerobic conditions. If one has a knowledge of the dose rate vs. time profile of a used fuel, the results and procedure presented here can be adopted to predict its dissolution rate as a function of time.

7. Summary and conclusions

Used nuclear fuel corrosion rates have been calculated assuming the instantaneous flooding with groundwater of a defective copper container occurs. The only significant source of oxidants in the failed copper container will be the radiolysis of water since the oxygen dissolved in the water will rapidly react with the copper walls of the container. The fuel dissolution rates are calculated as a function of the dose rate and cooling time at a temperature of 100°C, a conservative upper limit of the fuel temperature in the geological disposal vault. The rates decrease with time as radiation fields decrease. It is shown that for used CANDU fuel, the corrosion caused by alpha radiolysis is insignificant. The corrosion of the used fuel caused by beta and gamma radiolysis is important for $\sim$ 1000 a. Over this period $\sim$ 2% of the fuel will be dissolved.

Acknowledgements

We thank L.H. Johnson and F. King for helpful comments on the manuscript. In particular, we would like to thank F. King for help in the calculations for the rate of consumption of O_2 by Cu (Appendix A). The Canadian Nuclear Fuel Waste Management Program is jointly funded by AECL and Ontario Hydro under the auspices of the CANDU Owners Group (COG). AECL #1 1765.

Appendix A. Rate of consumption of the oxygen in the container by reaction with the fuel and/or the container

A.1. Consumption by reaction with fuel

Johnson [40] has conservatively estimated the fuel surface area to be ~ 2 cm^2 g^{-1} based on the determination of the particle size distribution of fuel fragments from a Bruce bundle. Each container in the vault will hold 72 fuel bundles each containing 21.3 kg of UO_2. Consequently, the total surface area of fuel exposable to water is 3.07×10^6 cm^2.

The consumption rate of O_2 by reaction with the fuel can then be calculated from the concentration of O_2 in the air-saturated water ($\sim 2 \times 10^{-4}$ mol l^{-1}) and the corrosion rate of UO_2 in aerated solution. We have used our electrochemical model to predict a rate of $\sim 2 \times 10^{-8}$ g d^{-1} cm^{-2} for the corrosion of UO_2 in aerated solution at $\sim$ 25°C [5]. Since the overall reaction for the consumption of O_2 by the corrosion of fuel

$$2UO_2 + O_2 + 2H_2O \rightarrow 2UO_2^{2+} + 4OH^- \qquad (A.1)$$

shows that two molecules of UO_2 are oxidized by each molecule of O_2, this leads to a consumption rate for O_2 of $\sim 1.3 \times 10^{-9}$ mol s^{-1}.

A.2. Consumption rate by reaction with copper

The consumption rate of O_2 by the copper container can be estimated using the mixed-potential model for copper corrosion published by King et al. [41]. In this model the mechanism assumed for the anodic dissolution of copper in saline solutions is

$$Cu + Cl^- \underset{k_{-1}}{\overset{k_1}{=}} CuCl + e^- \qquad (A.2)$$

$$CuCl + Cl^- \underset{k_{-2}}{\overset{k_2}{=}} CuCl_2^- \qquad (A.3)$$

where k_1, k_{-1}, k_2, k_{-2} are rate constants. The coupled cathodic reaction in this mechanism, the reduction of O_2, is

$$O_2 + 2H_2O + 4e^- \rightarrow 4OH^-. \qquad (A.4)$$

The results of King et al. show that Eq. (A.2) is fast and can be considered to be at equilibrium [41]. This means that the anodic reaction is mass-transport limited as opposed to the cathodic reaction (Eq. (A.4)) which is kinetically limited in aerated solution. By combining electrochemical expressions for the anodic and cathodic current densities with mass transport equations for steady-state diffusion, the corrosion current can be expressed in terms of the O_2 concentration by the expression

$$i_{corr}^3 = \frac{n_a F k_{ma} k_1 k_2 a_{Cl^-}^2}{k_{-1} k_{-2}} \left(n_c F k_c^0 [O_2]_0 \right)^2 \exp\left[\frac{F}{RT} \left(E_c^0 - E_a^0 \right) \right] \qquad (A.5)$$

which can be rewritten as

$$i_{corr} = \left(\frac{n_a F K}{k_{-2}} \left(n_c F k_c^0 [O_2]_0 \right)^2 \exp\left[\frac{F}{RT} \left(E_c^0 - E_a^0 \right) \right] \right)^{1/3}, \quad (A.6)$$

where

$$K = \frac{k_{ma} k_1 k_2 a_{Cl^-}^2}{k_{-1}} \quad (A.7)$$

which is appropriate when mass transport rates are high as will be the case inside the container. (By high we mean relative to the rates of mass transport in the compacted buffer/backfill material outside the container.) In these equations a_{Cl^-} is the activity of chloride in the groundwater, n_c is the number of electrons in the cathodic reaction, F is the Faraday constant, k_c^0 is the standard rate constant for Eq. (A.4), k_{ma} is the anodic mass transfer coefficient (5.5×10^{-5} cm s^{-1} for an assumed diffusion layer thickness of 0.1 cm), $[O_2]_0$ is the O_2 concentration in the flooded void space, R is the gas constant, T is the temperature, E_a^0 and E_c^0 are the standard potentials for Eqs. (A.2) and (A.4), respectively. It is clear from Eqs. (A.5) and (A.6) that i_{corr} will decrease with time as O_2 is depleted. We can calculate an initial value of i_{corr} (7×10^{-5} A cm^{-2}) from Eq. (A.5) using the value of $[O_2]_0$ for aerated solution (2×10^{-4} mol l^{-1}) and the values given by King et al. [41] for the other parameters. This is equivalent to a consumption rate for O_2 on the inside of the container (area 3.7×10^4 cm^2) of $\sim 1.3 \times 10^{-5}$ mol s^{-1}. This rate is 1×10^4 faster than the rate of consumption by fuel, and was calculated on the assumption that the reaction

$$Cu^+ \rightarrow Cu^{2+} + e^- \quad (A.8)$$

is fast in the solution and will use the same amount of oxygen as used for Eq. (A.2).

A.3. Time to consume all the oxygen

Given the large disparity in the rates of consumption of O_2, it is reasonable to assume that the great majority will be consumed by reaction with the copper container. An estimate of the time required to exhaust the available O_2 (t_{ex}) can be obtained by using a 'mean' value of i_{corr} ($(i_{corr})_m$) obtained from Eq. (A.5) using a value for $[O_2]_0$ equal to half the fully aerated value and the equation

$$t_{ex} = Q_{ox} n_c F / \left[(i_{corr})_m A_{Cu} \right] \quad (A.9)$$

where Q_{ox} is the initial quantity of O_2 present in the container (1.01 mol), and A_{Cu} is the surface area of the inside of the container (3.7×10^4 cm^2). This calculation shows that all the available O_2 in the container would be consumed by reaction with the container in ~ 1.4 days.

Appendix B. Sources of corrosion rates used in the model

Values of corrosion potentials measured as a function of dissolved O_2 concentration [5,42], gamma radiation dose rate [5,10,11] and alpha source strength [20] have been published. These values range from > 150 mV in solutions exposed to the highest gamma dose rates to < -200 mV for unirradiated deaerated solutions. As the current–potential relationship used in our model is based on data obtained with potentials ≥ 200 mV, it is clear that an extrapolation to the more positive corrosion potentials representative of oxidizing conditions will yield more reliable values of corrosion rate than the lengthy extrapolations to the negative end of the corrosion potential range measured under much less oxidizing conditions.

In Fig. 4 the corrosion rates obtained in this manner are plotted logarithmically as a function of the dose rate for both gamma and alpha radiation, and the lines represent linear fits to the data. While this fit appears to be reasonable, it obscures a number of features of the data. Fig. 9 shows a plot of the log of the corrosion rate against the square root of dose rate for the data recorded in the presence of gamma radiation. (Data in Fig. 9 do not contain the eight solid square points shown in Fig. 4, as discussed in Appendix C. It contains five data points at zero dose rates which cannot be shown in Fig. 4 due to the log scale used in this figure.) The square root of the dose rate is approximately proportional to the concentration of radiolysis products [35]. The solid line drawn in Fig. 9 shows that the logarithm of the corrosion rate is a linear function of the square root of dose rate for dose rates $\geq 1.6 \times 10^5$ Gy a^{-1}. The dashed lines are simply crude envelopes for the data.

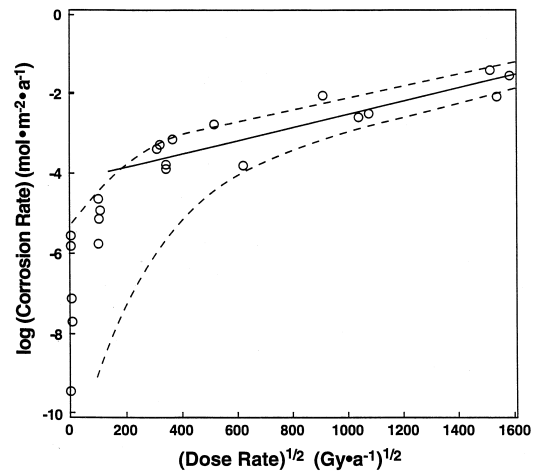

Fig. 9. Fuel corrosion rates (at 100°C) as a function of the square root of the gamma dose rate, using the data from Fig. 4. The solid line is a linear fit to the data points for dose rates $\geq 1.6 \times 10^5$ Gy a^{-1}. The dashed lines are envelopes for the data.

For lower dose rates, however, the dependence of corrosion rate on the concentration of radiolysis products appears to be unrealistically large, a fact that is obscured when the data are plotted logarithmically as in Fig. 4A. Our electrochemistry and XPS results show that this deviation from first order kinetics coincides with a change in the oxidation/dissolution mechanism of UO_2 [5,11]. In the linear region (dose rate $\geq 1.6 \times 10^5$ Gy a^{-1}) dissolution is occurring from an oxidized surface layer of composition $UO_{2.33}$. For dose rates $\geq 1.6 \times 10^5$ Gy a^{-1} the surface composition is a function of potential (UO_{2+x} with x decreasing as the potential decreases) and with decreasing dose rate less positive corrosion potentials are achieved [11]. The application of our electrochemical model, therefore, predicts corrosion rates that fall rapidly as the dose rate decreases.

It is possible that this predicted decrease in corrosion rate at low dose rates is real and can be taken to represent expected fuel behavior. However, it is also possible that extrapolation of currents measured at positive potentials [21,42] to corrosion potentials achieved in this region where the surface composition is potential-dependent is not merited; i.e., our electrochemical model no longer applies. Even if our model is still applicable, the length of the extrapolation needed to predict rates for low dose rates makes the values obtained uncertain. This uncertainty can be a few orders of magnitude as is clear from Fig. 4 for both gamma and alpha radiolysis. In the log fit used in Fig. 4, the weight of these low rates is increased with respect to the more accurate higher rates. For these reasons, the values plotted in Fig. 4 with closed symbols are not used in our predictions of fuel behavior.

The consequences of not using these data points lead to conservative predictions of corrosion rates at low dose rates since it assumes that the linear relationship observed at high dose rates will still apply as they decrease. This implicitly assumes that our electrochemical model established at potentials > -100 mV (vs. SCE) applies for potentials below this value also.

Appendix C. Determination of the fitting parameters for corrosion rates

By discarding the values for low dose rates (Fig. 4), we avoid predicting a major decrease in corrosion rate for used fuel at these low doses. This is particularly important for alpha radiolysis since we are predicting rates at dose rates substantially lower than those used experimentally (Fig. 5a). In the absence of a firm knowledge of the distribution of errors in the experimental points, it is difficult to decide what is the most appropriate relationship to use to fit the data and subsequently to extrapolate it. Consequently, we have performed least-square fits to the power-law dependence,

$$c = bd^a, \tag{C.1}$$

where c is the dissolution rate and d is the dose rate ($\alpha(t)$, $\beta(t)$ or $\gamma(t)$), both after a logarithmic transformation of the data points ('log fit') and directly for the original points ('direct fit'). The log fit corresponds to minimizing the following sum of residuals

$$\sum_i \left(\log c_i - \log\left(bd_i^a\right)\right)^2 \tag{C.2}$$

which is a linear problem both in log b and in a. The sum of residuals to minimize in the direct fit is

$$\sum_i \left(c_i - bd_i^a\right) \tag{C.3}$$

which results in a non-linear problem requiring a numerical solution of a single highly non-linear equation for the unknown a.

For alpha radiolysis we have used the log fit and estimated the error in a predicted value by calculating its standard deviation (Fig. 5a). This log fit was deemed more appropriate than a direct fit for two reasons. Firstly, values in a residuals plot are more symmetrically distributed around zero for the log fit than for the direct fit. (The residual plots for the alpha radiolysis look very similar to those for the gamma radiolysis, Figs. 10 and 11, as discussed below.) Secondly, the log fit effectively increases the weight of the low dose-rate points with respect to the high dose-rate points; this is appropriate since, for alpha radiolysis, we are always interpolating between the experimental points and zero dose rate (Fig. 5a).

For corrosion due to gamma/beta radiolysis a direct fit would be more conservative if an extrapolation to higher dose rates was required. (However, as for alpha radiolysis, the predominant need is for an extrapolation to lower dose rates.) For a direct fit of the gamma radiolysis data the residuals plot shows the typical triangular shape that war-

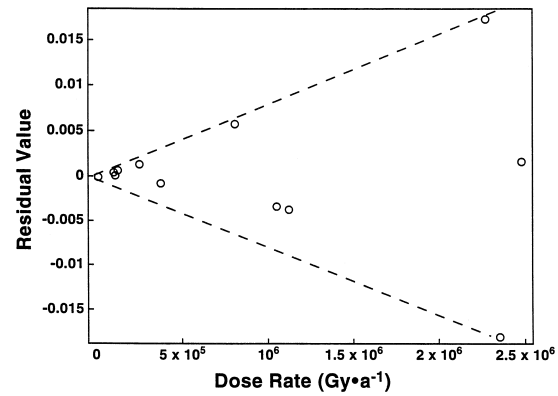

Fig. 10. Residuals plot for the least-square fit of the corrosion rates due to gamma radiolysis as a function of gamma dose rate (direct fit, data from Fig. 5b).

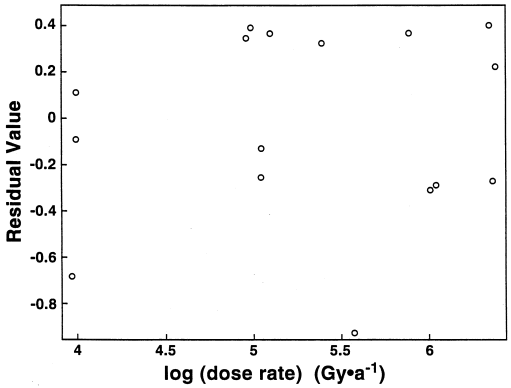

Fig. 11. Residuals plot for the least-square fit of the corrosion rates due to gamma radiolysis as a function of gamma dose rate after a logarithmic transformation of the data points (data from Fig. 5b).

rants a logarithmic transformation (Fig. 10), and the subsequent log fit yields a residuals plot with a more uniform distribution of values in a band of constant width about zero (Fig. 11).

This log fit yields a value for the slope of 1.86 ± 0.29 and would yield very conservative predictions of corrosion rates if extrapolated to higher dose rates. However, its extrapolation to lower dose rates will be particularly dependent on the accuracy of our experimental data points at lower dose rates. When deciding which data points were appropriate to fit, we discarded a number of points for low dose rates because they were corrosion rates predicted from low corrosion potentials in the region where the fuel surface composition is changing with potential. In this region our model may not apply, or, if it does, will yield corrosion rates which decrease rapidly with dose rate (Fig. 9). This is consistent with our understanding of the UO_2 oxidation/dissolution process. However, if the corrosion rate does decrease rapidly with dose rate for $d < 10^5$ Gy a^{-1} then the four points at $d \sim 10^4$ Gy a^{-1} (denoted by $\oplus$ in Fig. 4) are in error and grossly overpredict the rate for this dose rate. Their inclusion in our fit will, however, exert a significant influence on the slope since the log fit gives extra weight to these points, and a value for the slope of $\sim 1.39 \pm 0.12$ is obtained.

If the four data points ($\oplus$) are not included in our fit then a higher slope would be obtained and the extrapolation of this fit would predict lower corrosion rates at the lower dose rates than the extrapolation of the log fit when these data points are included. To avoid underestimating predicted corrosion rates at lower dose rates without excluding these points we have forced through the data of Fig. 5b a straight line of unit slope (Table 1). The straight line in Fig. 5b is the unforced fit (slope ~ 1.39) to illustrate the conservatism inherent in the forced fit procedure.

References

[1] L.H. Johnson, D.W. Shoesmith, Spent Fuel, in: W. Lutze, R.C. Ewing (Eds.), Radioactive Waste Forms for the Future, Elsevier, Amsterdam, 1988, p. 635.
[2] B. Grambow, Used Fuel Dissolution and Oxidation, An Evaluation of Literature Data, SKB Technical Report, SKB 89-13, 1989.
[3] H. Christensen, R.S. Forsyth, R. Lundqwist, L.O. Werme, Radiation-Induced Dissolution of UO_2, Studsvik Report, NS-90/85, Studsvik Nuclear, Nykoping, Sweden, 1990.
[4] S. Sunder, D.W. Shoesmith, Chemistry of UO_2 Fuel Dissolution in Relation to the Disposal of Used Nuclear Fuel, Atomic Energy of Canada Limited Report, AECL-10395, 1991. [1]
[5] D.W. Shoesmith, S. Sunder, An Electrochemistry-Based Model for the Dissolution of UO_2, Atomic Energy of Canada Limited Report, AECL-10488, 1991.
[6] J. Bruno, I. Casas, I. Puigdomènech, Geochim. Cosmochim. Acta 5S (1991) 647.
[7] SKB (Swedish Nuclear Fuel and Waste Management Co.), SKB91, Final Disposal of Spent Nuclear Fuel, Importance of the Bedrock for Safety, Swedish Nuclear Fuel and Waste Management Company Report, SKB-TR-92-20, 1992.
[8] R.S. Forsyth, L.O. Werme, J. Nucl. Mater. 190 (1992) 3.
[9] W.J. Gray, H.R. Leider, S.A. Steward, J. Nucl. Mater. 190 (1992) 46.
[10] D.W. Shoesmith, S. Sunder, J. Nucl. Mater. 190 (1992) 20.
[11] S. Sunder, D.W. Shoesmith, H. Christensen, N.H. Miller, J. Nucl. Mater. 190 (1992) 78.
[12] Hj. Matzke, J. Nucl. Mater. 190 (1992) 101.
[13] S. Sunder, D.W. Shoesmith, N.H. Miller, G.J. Wallace, in: C.F. Sombret (Ed.), Materials Research Society Symposia Proceedings, vol. 257, Scientific Basis for Nuclear Waste Management XV, 1992, p. 345.
[14] S. Sunder, H. Christensen, Nucl. Technol. 104 (1993) 403.
[15] H. Christensen, S. Sunder, D.W. Shoesmith, J. Alloys Compounds 213&214 (1994) 93.
[16] L.H. Johnson, J.C. Tait, D.W. Shoesmith, J.L. Crosthwaite, M.N. Gray, The Disposal of Canada's Nuclear Fuel Waste: Engineered Barriers Alternatives, Atomic Energy of Canada Limited Report, AECL-10718, COG-93-8, 1994.
[17] L.H. Johnson, D.M. LeNeveu, D.W. Shoesmith, D.W. Oscarson, M.N. Gray, R.J. Lemire, N.C. Garisto, The Disposal of Canada's Nuclear Fuel Waste: The Vault Model for Postclosure Assessment, Atomic Energy of Canada Limited Report, AECL-10714, COG-93-4, 1994.
[18] B. Grambow, A. Loida, P. Dressler, H. Geckeis, P. Diaz, J. Gago, I. Casas, J. de Pablo, J. Gimenez, M.E. Torrero, Long-term Safety of Radioactive Waste Disposal: Reaction of High Burnup Spent Fuel and UO_2 in Saline Brines at Room Temperature, Kernforschungszentrum Karlsruhe Report, KfK 5377, 1994.
[19] W.J. Gray, L.E. Thomas, in: A. Barkatt, R.A. Van Konynenburg (Eds.), Materials Research Society Symposia Proceed-

[1] Atomic Energy of Canada Limited Report, available through SDDO, Chalk River Laboratories, Chalk River, Ontario, Canada K0J 1J0.

ings, vol. 333, Scientific Basis for Nuclear Waste Management XVII, 1994, p. 391.
[20] S. Sunder, D.W. Shoesmith, N.H. Miller, in: T. Murakami, R.C. Ewing (Eds.), Materials Research Society Symposia Proceedings, vol. 353, Scientific Basis for Nuclear Waste Management XVIII, 1995, p. 617.
[21] S. Sunder, L.K. Strandlund, D.W. Shoesmith, Anodic Dissolution of UO_2 in Slightly Alkaline Sodium Perchlorate Solutions, Atomic Energy of Canada Limited Report, AECL-11440, COG-95-461, 1996.
[22] D.W. Shoesmith, J.C. Tait, S. Sunder, W.J. Gray, S.A. Steward, R.E. Russo, J.D. Rudnicki, Factors Affecting the Differences in Reactivity and Dissolution Rates Between UO_2 and Spent Nuclear Fuels, Atomic Energy of Canada Limited Report, AECL-11515, COG-95-581, 1996.
[23] B. Grambow, A. Loida, P. Dressler, H. Geckeis, P. Diaz, J. Gago, I. Casas, J. de Pablo, J. Gimenez, M.E. Torrero, Long-term Safety of Radioactive Waste Disposal: Chemical Reaction of Fabricated and High Burnup Spent UO_2 Fuel With Saline Brines, Kernforschungszentrum Karlsruhe Report, KfK 5702, 1996.
[24] L.H. Johnson, D.M. Leneveu, F. King, D.W. Shoesmith, M. Kolar, D.W. Oscarson, S. Sunder, C. Onofrei, J.L. Crosthwaite, The Disposal of Canada's Nuclear Fuel Waste: A Study of Post-closure Safety of In-room Emplacement of Used CANDU Fuel in Copper Containers in Permeable Plutonic Rock, vol. 2, Vault Model, Atomic Energy of Canada Limited Report, AECL-111494-2, COG-95-552-2, 1996.
[25] G.L. Doubt, Assessing Reliability and Useful Life of Containers for Disposal of Irradiated Fuel Waste, Atomic Energy of Canada Limited Report, AECL-8328, 1984.
[26] M.D.C. Moles, Copper Inspection Issues for Nuclear Used Fuel Container Final Closure Welds, Ontario Hydro Research Division Report, M92-50-K, 1992.
[27] R.J. Lemire, F. Garisto, The solubility of U, Np, Pu, Th and Tc in a Geological Disposal Vault for Used Nuclear Fuel, Atomic Energy of Canada Limited Report, AECL-10009, 1989.
[28] D.W. Shoesmith, S. Sunder, W.H. Hocking, in: J. Lipkowski, P.N. Ross (Eds.), Electrochemistry of Novel Materials, VCH, New York, 1994, p. 297.
[29] F. Garisto, Ann. Nucl. Energy 16 (1989) 33.
[30] S. Sunder, Alpha, Beta and Gamma Dose Rates in Water in Contact with Used CANDU UO_2 Fuel, Atomic Energy of Canada Limited Report, AECL-11380, COG-95-340, 1995.
[31] A.O. Allen, The Radiation Chemistry of Water and Aqueous Solutions, Van Nostrand, Princeton, NJ, 1961.
[32] J.W.T. Spinks, R.J. Woods, An Introduction to Radiation Chemistry, 3rd ed., Wiley-Interscience, New York, 1990.
[33] M. Kolar, F. King, in: W.M. Murphy, D. Knecht (Eds.), Materials Research Society Symposia Proceedings, vol. 412, Scientific Basis for Nuclear Waste Management XIX, 1996, p. 547.
[34] R.J. McEachern, A review of kinetic data on the rate of U_3O_7 formation on UO_2, J. Nucl. Mater., in press.
[35] H. Christensen, S. Sunder, Calculations of Radiolysis in Connection with UO_2 Oxidation Studies, Studsvik Nuclear Technical Note, NS-89/117, 1989.
[36] D.W. Shoesmith, S. Sunder, M.G. Bailey, N.H. Miller, J. Nucl. Mater. 227 (1996) 287.
[37] P. Baumgartner, Alternative Postclosure Assessment: Disposal Container Surface and Centre Temperature History, Technical memoranda, GSEB-95-322, GSEB-95-328, 1995.
[38] R.S.C. Wai, A. Tsai, Three Dimensional Thermal and Thermal–mechanical Analyses for a Used-fuel Disposal Vault with the In-room Emplacement Option, Ontario Hydro Report No. N-REP-03780-0083 R00, 1995.
[39] J.J. Cramer, J.A.T. Smellie, Final Report of the AECL/SKB Cigar Lake Analog Study, Atomic Energy of Canada Limited Report, AECL-10851, COG-93-147, SKB TR-94-04, 1994.
[40] L.H. Johnson, The Dissolution of Irradiated UO_2 Fuel in Groundwater, Atomic Energy of Canada Limited Report, AECL-6837, 1982.
[41] F. King, C.D. Litke, M.J. Quinn, D.M. Leneveu, Corros. Sci. 37 (5) (1995) 833.
[42] D.W. Shoesmith, S. Sunder, M.G. Bailey, G.J. Wallace, Corros. Sci. 29 (1989).